

# Far Ultraviolet Spectral Images of the Vela Supernova Remnant

K. Nishikida<sup>1</sup>, J. Edelstein<sup>1</sup>, E. J. Korpela<sup>1</sup>, R. Sankrit<sup>1</sup>, W. M. Feuerstein<sup>1</sup>, K. W. Min<sup>2</sup>, J-H. Shinn<sup>2</sup>, D-H. Lee<sup>2</sup>, I-S. Yuk<sup>3</sup>, H. Jin<sup>3</sup>, K-I. Seon<sup>3</sup>

## ABSTRACT

We present far-ultraviolet (FUV) spectral-imaging observations of the Vela supernova remnant (SNR), obtained with the Spectroscopy of Plasma Evolution from Astrophysical Radiation (*SPEAR*) instrument, also known as *FIMS*. The Vela SNR extends  $\sim 8^\circ$  in the FUV and its global spectra are dominated by shock-induced emission lines. We find that the global FUV line luminosities can exceed the 0.1–2.5 keV soft X-ray luminosity by an order of magnitude. The global O VI:C III ratio shows that the Vela SNR has a relatively large fraction of slower shocks compared with the Cygnus Loop.

*Subject headings:* ISM: individual (Vela Supernova Remnant) – supernova remnants – ultraviolet: ISM

## 1. Introduction

The Vela supernova remnant (SNR) has been studied in great detail due to its proximity (250pc; Cha et al. 1999) and its large angular diameter of  $8^\circ$  (Aschenbach et al. 1995). The remnant is  $\sim 10,000$  years old (Reichley et al. 1970) and its overall emission is dominated by the interaction of the SN blast wave with the interstellar medium (ISM), but also has a pulsar and plerionic nebula near its center.

Vela is one of two Galactic SNRs (the other being the Cygnus Loop) that has been extensively studied in the UV. The UV emission from SNRs arises primarily in shocks driven by the supernova blast wave into interstellar clouds. The shock velocities responsible for the UV emission lie in the range  $\sim 50\text{--}300$  km s<sup>-1</sup>, and heat the gas to temperatures of  $10^5 - 10^6$  K. The hot shocked gas can also be studied via absorption so long as there are suitable background continuum sources.

Absorption line studies of Vela using *Copernicus* showed the presence of O VI and N V, high ionization species expected in shocked gas, and also high velocity components of lower ionization species (Jenkins et al. 1976a,b). Absorption line studies have also been carried out with *IUE* (Jenkins et al. 1984; Nichols & Slavin 2004), *HST* (Jenkins & Wallerstein 1995; Jenkins et al. 1998)

---

<sup>1</sup>Space Sciences Laboratory, University of California, Berkeley, CA 94720

<sup>2</sup>Korea Advanced Institute of Science and Technology, 305-701, Daejeon, Korea

<sup>3</sup>Korea Astronomy and Space Science Institute, 305-348, Daejeon, Korea

and *FUSE* (Slavin et al. 2004). These studies have shown the existence of fast shocks ( $\gtrsim 160 \text{ km s}^{-1}$ ) distributed widely but inhomogeneously across the face of the remnant, and also the variations in the dynamic pressure driving these shocks.

Emission line studies of Vela have been carried out using *IUE* (Raymond et al. 1991), *HUT* (Raymond et al. 1997), *FUSE* (Sankrit et al. 2001, 2003) and *Voyager 2* UVS (Blair et al. 1995, henceforth BVL). These observations, except for the ones obtained by *Voyager 2*, were of regions with angular extents of order an arc-minute and probed the properties of individual shock fronts. BVL analyzed *Voyager 2* spectra of a  $1.5^\circ \times 2.0^\circ$  region in the northern part of Vela, which showed strong C III and O VI emission features. They found variations in the flux ratios on scales of  $0.2^\circ$ . They also concluded from the overall flux ratio between the two lines that slower shocks (those unable to produce O VI) were more prevalent in Vela than in the Cygnus Loop. *FUSE* spectra of a few regions in Vela well separated from each other have strong C III lines and relatively weak or no O VI, and show the presence of slower shocks ( $100 - 140 \text{ km s}^{-1}$ ) spread over the face of the remnant (Sankrit 2004).

We present spectral images of the Vela SNR in several FUV lines and FUV spectra of the entire remnant. The data were obtained with *SPEAR* (The Spectroscopy of Plasma Emission from Astrophysical Radiation), also known as *FIMS* (Far-ultraviolet Imaging Spectrograph). *SPEAR*, launched September 27, 2003 on the Korean satellite STSAT-1, is a dual-channel FUV imaging spectrograph (S channel 900 - 1150 Å, L channel 1350 - 1750 Å,  $\lambda/\Delta\lambda \sim 550$ ) with a large imaged field of view (S:  $4.0^\circ \times 4.6'$ , L:  $7.5^\circ \times 4.3'$ , spatial resolution  $\sim 10'$ ) optimized for the observation of diffuse emission (see Edelman et al. 2005a,b, for an overview of the instrument and mission). A large effective field of view can be obtained by sweeping across the sky. This combination of instrument properties yields a dataset that supplements data obtained in previous UV studies of the remnant. The data allow us to estimate the total flux from Vela in several FUV lines.

In the following sections we present the observations (§2), discuss the spectral images (§3) and the total spectrum (§4). The last section (§5) summarizes the importance of these data for the study of SNRs.

## 2. Observation and Data Analysis

The Vela SNR region was observed between January 31 and February 4, 2004. The data were processed as described in Edelman et al. (2005a,b) including rejection of data for which the attitude knowledge was poor ( $>30'$ ) or data contaminated by airglow, evident from an increased count rate at the end of each orbit ( $\leq 10\%$  of the data). The resulting number of photons and exposure obtained over 16 orbits were ( $4.4 \times 10^6$ , 7214 s) and ( $1.8 \times 10^5$ , 6307 s) for the L channel and S channel, respectively. While the SNR region was entirely observed in the L channel, the S channel coverage was incomplete. The photon's sky coordinates ( $\alpha$ ,  $\delta$ ) and wavelengths ( $\lambda$ ) were binned to  $0.15^\circ$  (similar to the *SPEAR* imaging resolution after attitude reconstruction) and to 1

Å, respectively and combined with exposure maps to create a 3-d count-rate data cube ( $\alpha$ ,  $\delta$ ,  $\lambda$ ) for each spectral channel. We identified data contaminated by bright stars in each channel as pixels in the wavelength-integrated total count rate image that exceeded 3 times the median count rate of a relatively star-free area. The L and S channels contained 20% and 10% of the total pixels identified as stars, respectively.

To create spectral images, the data cube was summed across the waveband of interest with star pixels removed. Star pixel “holes” were filled with a linear fit to adjacent pixels at the “hole’s” declination. The undetected stars have a flux  $< 1.5 \times 10^{-11}$  ergs s $^{-1}$  cm $^{-2}$ Å $^{-1}$  in the *SPEAR* L channel. Improved stellar identification, removal and reconstruction methods are currently being developed.

Net spectral images for specific emission lines,  $I_{\lambda_{Net}}$ , were constructed by subtracting a continuum image,  $I_{cont}$ , made from a similar width spectral region *adjacent* to the emission line from an image,  $I_{\lambda}$ , made from a spectral region *including* the emission line, i.e.  $I_{\lambda_{Net}} = I_{\lambda} - I_{cont}$ . This approach often results in an over-subtraction of the lower intensity pixels. The continuum selected from the global spectra is not suitable for lower intensity pixels because of the non-zero slope of the adjacent continuum. Therefore we apply a variable scaling factor,  $f$ , to the subtraction of the continuum image:  $I_{\lambda_{Net}} = I_{\lambda} - f \times I_{cont}$ . For each line image, the factor  $f$  was set for each image pixel associated with a bin of a five-bin intensity histogram of  $I_{\lambda}$  such that 70% (i.e.  $\sim 2\sigma$ ) of those pixels would have a net positive flux. The resulting values of  $f$  were 1.0 at high to medium intensity bins and decreased for the lowest one to three intensity bins, depending on  $\lambda$ , with a typically minimum value of  $f = 0.6$  for the lowest intensity bin. The resulting  $I_{\lambda_{Net}}$  were smoothed using a 3-pixel ( $0.45^\circ$ ) square median smoothing function. Diffuse spectra were derived by totaling photons and exposure over regions of interest, excluding bright star pixels, and then smoothed by a 3 Å boxcar function.

### 3. Spectral Images

We show the C IV (1543–1557 Å) image of Vela in Fig. 1. This is the most prominent emission line in the L channel, and the figure shows the overall morphology of the FUV emission from the SNR. Images of Vela in C III (974–980 Å), O VI (1019–1033 Å), Si IV & O IV] (1398–1413 Å) are shown in Fig. 2. Also shown for comparison is the *ROSAT* All-Sky Survey (RASS) 1/4 keV image of the same region. The *SPEAR* maps show that FUV emission is present over most of the Vela SNR. The C III map in particular shows the widespread presence of radiative shocks. O VI and C III trace gas at very different ionization states. O VI production requires a shock velocity of about 150 km/s while C III is produced even in 80 km/s shocks. There is some overall correspondence between the two, showing where the FUV producing shocks exist, but C III is more extended. C IV and Si IV & O IV] images show a close correlation: C IV, Si IV, and O IV] have comparable ionization potentials and are roughly co-extensive in the post-shock gas.

Although the FUV and X-ray emission features are not closely correlated, their extent is roughly the same. Lu & Aschenbach (2000) attribute the X-ray emission to thermal emission from a hot, thin gas in the SNR interior. We used the plasma temperatures and emission measures in Table 1 of Lu & Aschenbach (2000) as input for CHIANTI (Dere et al. 1997; Young et al. 2003) and confirmed that they produce insufficient thermal FUV emission by several orders of magnitudes compared with the observed emission. The FUV emission comes from shocks that have been driven into interstellar clouds. These clouds are large enough that they have not been destroyed by the blast wave sweeping over them, and they have a high covering factor. The total FUV luminosity of Vela exceeds the total soft X-ray luminosity (see §4). Thus, the overall radiation rate of the SNR is dominated by shocks in higher density regions traced by their FUV emission.

The most prominent localized feature is an intense knot of emission near  $(\alpha, \delta)=(8.6 \text{ h}, -42.5^\circ)$  that appears at all FUV wavelengths, including the soft X-ray band. A detailed comparison shows that the peak emission for each FUV wavelength and the soft X-ray are non-coincident and arranged in an arc, suggesting that the feature could be a complex and intense bow shock perhaps analogous to the X-ray “bullet shocks,” or “knots,” of similar scale. Aschenbach et al. (1995) identified six (labeled A through F) of these X-ray knots and suggested that they were created by high-density ejecta shock-heating the ambient medium. The FUV images appear to be limb brightened along the north-east shell boundary and, notably, joins the X-ray knot D to the main shell in C IV and Si IV/O IV].

FUV emission is absent from the knot B region despite its similarity in X-ray intensity to knot D. This is consistent with FUV emission arising from shocked interstellar media because the knot D bullet is believed to be encountering a more dense ambient media than knot B. An FUV enhancement particularly notable in O VI, whose localized intensity peak is coincident with the Vela pulsar, and C III, which coincides with the Vela-X radio continuum nebula (Haslam et al. 1982; Bock et al. 1998, Figures 1 & 2), is coincident with a soft X-ray ridge, suggestive of a shock structure. Curiously, there is little associated C IV or Si IV & O IV] emission from the same area in comparison to the region of maximum intensity  $(\alpha, \delta)=(8.6 \text{ h}, -42.5^\circ)$ . This suggests that we are detecting at least two markedly different physical conditions in the region surrounding the Vela pulsar. A more detailed examination will be necessary to tell if these are related, or merely happen to lie along the same line of sight.

#### 4. FUV Spectra

The diffuse *SPEAR* FUV spectra from the entire Vela SNR region are shown in Fig. 3. The spectra show strong emission lines from highly ionized atoms produced by high velocity shocks and/or hot plasmas. Detected lines include C III (977 Å), N III (990 Å), O VI (1032, 1038 Å), O IV] and Si IV (1400, 1403 Å unresolved), N IV (1486 Å), C IV (1548, 1550 Å), He II (1640 Å), and O III] (1660, 1666 Å). The emission line-like feature near 1695 Å is instrumental.

Table 1 shows the observed FUV line intensities averaged over the SNR. The C IV, He II, and O III] line profiles were fitted with a Gaussian line profile and a local linear background, while the C III and O VI 1032 Å lines required an additional Gaussian line profile to fit airglow lines adjacent to C III and O VI  $\lambda$ 1032. The O VI doublet intensity was calculated by multiplying the 1032 Å line intensity by 1.5 (assuming a 2:1 ratio between  $\lambda$ 1032, 1038) since *SPEAR* does not have the spectral resolution necessary to resolve O VI  $\lambda$ 1038 and C II\*  $\lambda$ 1037. For C III and O VI, we assumed that the average intensity calculated from areas with sky coverage applied to the entire SNR. Since the Vela SNR appears to be faint at the edges, it is likely that the intensities are slightly overestimated. The estimated systematic uncertainty in the *SPEAR* sensitivity is  $\sim 25\%$  (Edelstein et al. 2005a). The *Voyager 2* UVS measurements of O VI and C III line intensities at 28 Å resolution (BVL) are in agreement within a factor of two below *SPEAR* measurements in an area near ( $\pm 1^\circ$ ) UVS pointings. The global observed O VI:C III ratio is  $\sim 1$ , consistent within a factor of about two (both above and below) reported by BVL.

We apply multiplicative correction factors (shown in Table 1) to the observed global FUV luminosities, presuming a diameter of  $8^\circ$  and distance of 250 pc, to derive dereddened luminosities. These correction factors were calculated by Sankrit et al. (2003) by assuming  $R=3.1$  for selective extinction,  $E(B-V)=0.1$  (Wallerstein & Balick 1990), and using the extinction curve suggested by Fitzpatrick (1999). The integrated C III or O VI line luminosity can exceed the entire 0.1 - 2.5 keV luminosity,  $2.2 \times 10^{35}$  ergs  $s^{-1}$  (Lu & Aschenbach 2000), by more than an order of magnitude, confirming the importance of the FUV waveband to SNR cooling.

Vela’s global FUV luminosity can be compared with that of the Cygnus Loop (Blair et al. 1991). Vela is about five times less luminous than Cygnus in the X-ray and in C IV, about twice as faint in O VI, and is equally as luminous in C III. The observed O VI:C III ratio of Cygnus is  $\sim 2$ , illustrating the relatively large fraction of slower shocks in Vela compared with Cygnus. For Cygnus, Rasmussen & Martin (1991) showed that the O VI luminosity is at least as much as the 0.1–4 keV X-ray luminosity (Ku et al. 1984); the combined O VI, C III, C IV luminosity was found to be ten times as large as the X-ray luminosity (Blair et al. 1991). In both the Cygnus Loop and Vela, the supernova blast wave is expanding into inhomogeneous surroundings, and the radiative shocks in the denser interaction regions emit strongly in the FUV.

## 5. Summary and Future Work

We have presented global FUV spectral images and spectra of the Vela SNR. Our data indicate inhomogeneous shock-induced emission from the SNR surface. The images show limb brightening and knots of emission. The spectra are consistent with past FUV observations of Vela. The global FUV luminosities of emission lines can exceed the soft X-ray luminosity by an order of magnitude, providing an efficient cooling channel to the SNR.

The data will be used to compare the global FUV morphology with images in other wavebands

and examine how the SNR evolves and interacts with the ambient ISM. *SPEAR* spectra toward previously observed regions (ex. Raymond et al. 1997; Sankrit et al. 2001) will be modeled in detail to determine the physical properties of the regions. Mapping the O VI:C III ratio will allow us to map the distribution of shock velocities across Vela. Furthermore, the global *SPEAR* spectra can be compared with those of neighboring regions to investigate Vela’s association with the Gum nebula.

*SPEAR / FIMS* is a joint project of KASSI & KAIST (Korea) and U.C., Berkeley (USA), funded by the Korea MOST and NASA Grant NAG5-5355. We used NASA’s *SkyView* (<http://skyview.gsfc.nasa.gov>) facility and CHIANTI, a collaboration of NRL (USA), RAL (UK), U. Florence (Italy) and Cambridge (UK).

## REFERENCES

- Aschenbach, B., Egger, R., & Trümper, J. 1995, *Nature*, 396, 587
- Blair, W. P., Long, K. S., Vancura, O., & Holberg, J. B. 1991, *ApJ*, 374, 202
- Blair, W. P., Vancura, O., & Long, K. S. 1995, *AJ*, 110, 312
- Bock, D. C.-J., Turtle, A. J., & Green, A. J. 1998, *AJ*, 116, 1886
- Cha, A. N., Sembach, K. R., & Danks, A. C. 1999, *ApJ*, 515, L25
- Dere, K. P., Landi, E., Mason, H. E., Monsignori Fossi, B. C., & Young, P. R. 1997, *ApJS*, 125, 149
- Edelstein, J., Korpela, E. J., Adlofo, J., Bowen, M., Feuerstein, W. M., Hull, J., Jelinsky, S., Nishikida, K., McKee, K., Berg, P., Chung, R., Fischer, J., Min, K. W., Oh, S.-H., Rhee, J.-G., Ryu, K., Shinn, J.-H., Han, W., Lee, D.-H., Seon, K.-I., Jin, H., Yuk, I.-S., Park, J.-H., & Nam, U.-W. 2005a, *ApJ*, submitted
- Edelstein, J., Min, K. W., Han, W., Korpela, E. J., Nishikida, K., Welsh, B. Y., Heiles, C., Feuerstein, W. M., Adlofo, J., Bowen, M., McKee, K., Lim, J.-T., Ryu, K., Shinn, J.-H., Nam, U.-W., Park, J.-H., Yuk, I.-S., Jin, H., Seon, K.-I., Lee, D.-H., & Sim, E. 2005b, *ApJ*, submitted
- Fitzpatrick, E. L. 1999, *PASP*, 111, 63
- Haslam, C. G. T., Stoffel, H., Salter, C. J., & Wilson, W. E. 1982, *A&AS*, 47, 1
- Jenkins, E. B., Tripp, T. M., Fitzpatrick, E. L., Lindler, D., Danks, A. C., Beck, T. L., Bowers, C. W., Joseph, C. L., Kaiser, M. E., Kimble, R. A., Kraemer, S. B., Robinson, R. D., Timothy, J. G., Valenti, J. A., & Woodgate, B. E. 1998, *ApJ*, 492, L147

- Jenkins, E. B. & Wallerstein, G. 1995, *ApJ*, 440, 227
- Jenkins, E. B., Wallerstein, G., & Silk, J. 1976a, *ApJ*, 209, L87
- . 1976b, *ApJS*, 32, 681
- Jenkins, E. B., Wallerstein, G., & Silk, J. 1984, *ApJ*, 278, 649
- Ku, W. H.-M., Kahn, S. M., Pisarski, R., & Long, K. S. 1984, *ApJ*, 278, 615
- Lu, F. J. & Aschenbach, B. 2000, *A&A*, 362, 1083
- Nichols, J. S. & Slavin, J. D. 2004, *ApJ*, 610, 285
- Rasmussen, A. & Martin, C. 1991, *ApJ*, 396, 103L
- Raymond, J. C., Blair, W. P., Long, K. S., Vancura, O., Edgar, R. J., Morse, J., Hartigan, P., & Sanders, W. T. 1997, *ApJ*, 482, 881
- Raymond, J. C., Wallerstein, G., & Balick, B. 1991, *ApJ*, 383, 226
- Reichley, P. E., Downs, G. S., & Morris, G. A. 1970, *ApJ*, 159, L35
- Sankrit, R. 2004, in Proceedings of the conference “How Does The Galaxy Work?”, ed. E. J. Alfaro, E. Perez, & J. Franco (Dordrecht; London; Kluwer Academic), 177
- Sankrit, R., Blair, W. P., & Raymond, J. C. 2003, *ApJ*, 587, 242
- Sankrit, R., Shelton, R. L., Blair, W. P., Sembach, K. R., & Jenkins, E. B. 2001, *ApJ*, 549, 416
- Slavin, J. D., Nichols, J. S., & Blair, W. P. 2004, *ApJ*, 606, 900
- Wallerstein, G. & Balick, B. 1990, *MNRAS*, 245, 701
- Young, P. R., Del Zanna, G., Landi, E., Dere, K. P., Mason, H. E., & Landini, M. 2003, *ApJS*, 144, 135

Table 1: Observed global FUV intensities and dereddened luminosities of the Vela SNR

| Species   | C III | O VI | C IV | He II | O III] | X-ray |
|---|-------|------|------|-------|--------|-------|
| Observed intensity ( $10^5 LU$ )                  | 2.6   | 2.7  | 2.3  | 0.5   | 0.5    |       |
| Reddening correction                              | 4.47  | 3.73 | 2.07 | 2.03  | 2.03   |       |
| Dereddened luminosity ( $10^{35}$ ergs $s^{-1}$ ) | 26.8  | 22.7 | 8.0  | 1.3   | 1.5    | 2.2   |

Note. — Diameter of  $8^\circ$  and 250 pc distance assumed. The O VI luminosity was calculated assuming a 2:1 line ratio between O VI 1032 Å and 1038 Å lines. Reddening correction values are taken from Sankrit et al. (2003). X-ray (0.1–2.5 keV) luminosity from Lu & Aschenbach (2000). 1 Line Unit (LU) = 1 photon  $s^{-1}$   $cm^{-2}$   $sr^{-1}$  =  $1.9 \times 10^{-11}$  ergs  $s^{-1}$   $cm^{-2}$   $sr^{-1}$  at 1032 Å and  $1.3 \times 10^{-11}$  ergs  $s^{-1}$   $cm^{-2}$   $sr^{-1}$  at 1550 Å.



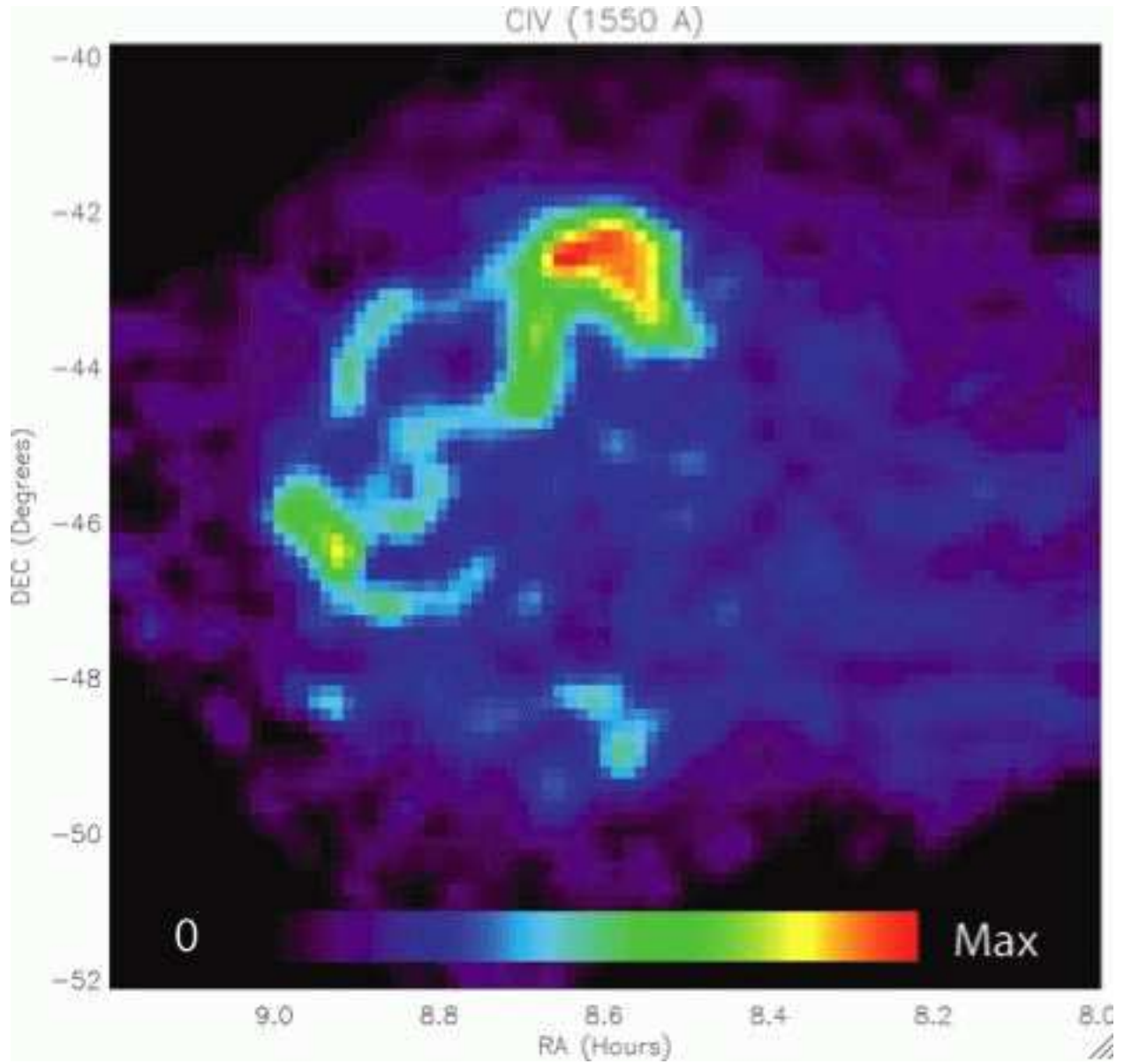


Fig. 1.— *SPEAR* C IV image of the Vela SNR. Intensity scale (linear), which applies to the *SPEAR* images in Fig. 2 as well, is also shown. Maximum intensity of the C IV image is  $1.7 \times 10^6$  LU.

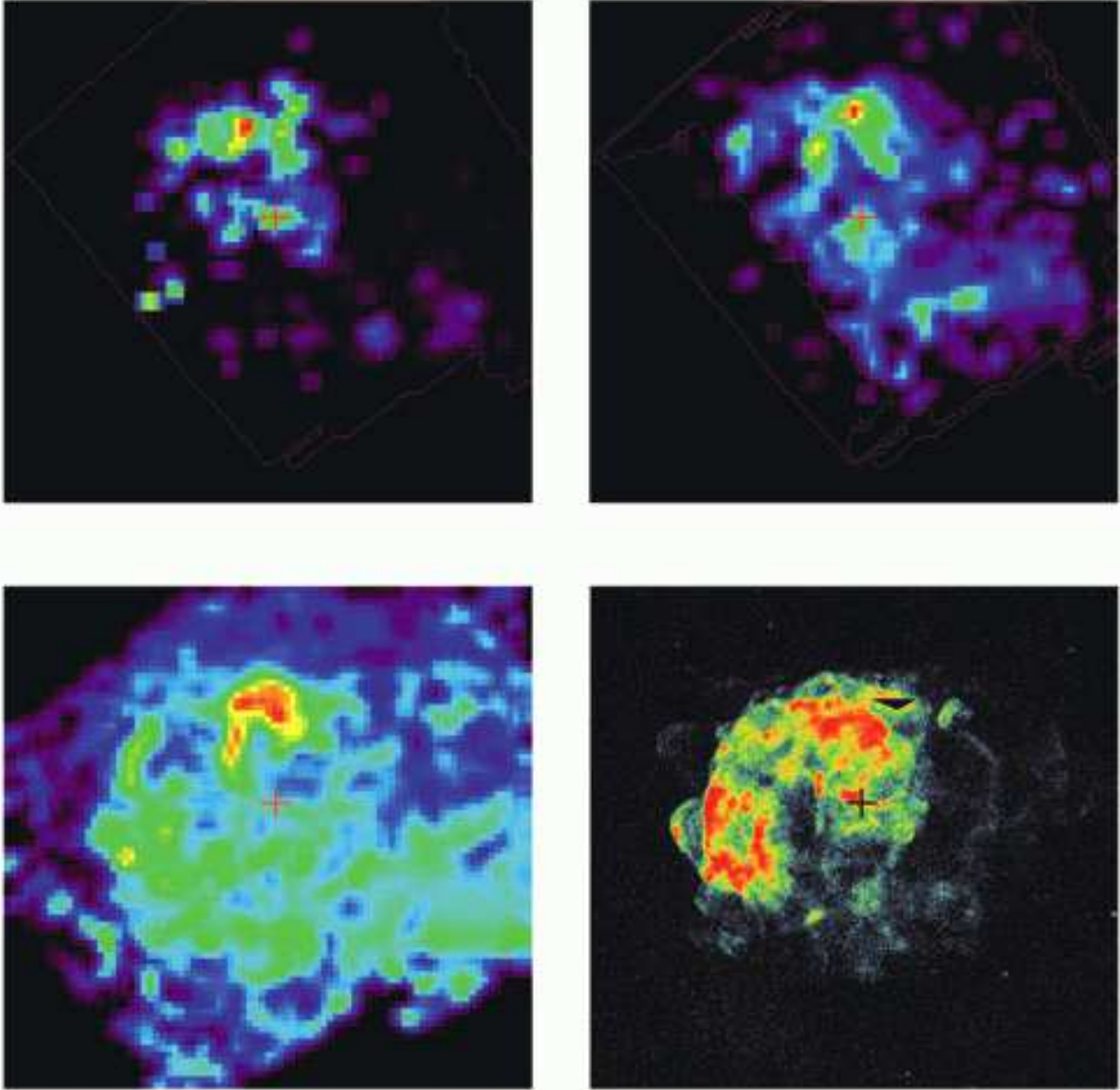


Fig. 2.— Top row: *SPEAR* O VI (left) and C III (right) images. Observation boundary is shown in both images. The inner contour shown in the C III image corresponds to 15% of the maximum exposure in the S channel. Bottom row: Si IV & O IV (left) and RASS 1/4 keV (right) images. The “+” symbol indicates the position of the Vela pulsar. Maximum intensities (in  $10^6$  LU) seen in the O VI, C III, and Si IV & O IV] images are 2.9, 4.1, and 0.62, respectively.

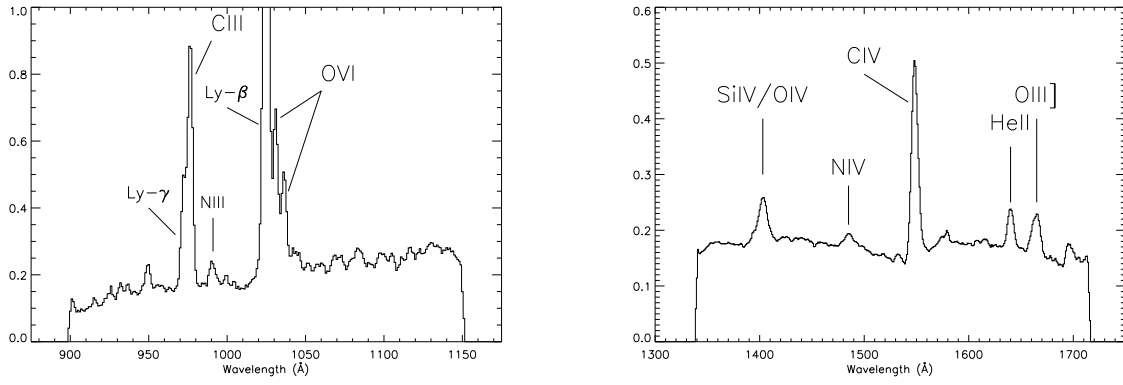


Fig. 3.— The average Vela spectra as obtained with *SPEAR*. Vertical axis is in units of  $10^5 \text{ photons s}^{-1} \text{ cm}^{-2} \text{ sr}^{-1} \text{ \AA}^{-1}$ . In addition to Ly- $\beta$  and Ly- $\gamma$ , the higher hydrogen Lyman series can be seen between 910 Å and 950 Å. The Lyman series is due to geocoronal emission.